Journal for
Electrochemistry and
Plating Technology

JEPT

Edited by: DGO-Fachausschuss Forschung – Hilden / Germany

A new insight into the phosphorus distribution of nanocrystalline Ni-Ni_3P-diamond composites

The microstructure of an electroplated Ni-Ni_3P-diamond composite has been studied by field-emission scanning electron microscopy, energy dispersive X-ray spectrometry and transmission Kikuchi diffraction. The use of an electron transparent sample reduced the resolution limits of X-ray spectrometry and electron backscatter diffraction. Basing on the P distribution and Ni/Ni_3P orientation maps, standard observations made by backscattered electron imaging can be easily interpreted.

Received: 2013-04-04
Received in revised form: 2013-04-05
Accepted: 2013-04-08

Keywords: Ni-P diamond coatings, phosphorus distribution, transmissions Kikuchi diffraction, electron backscatter imaging

By D. Dietrich, A. Sadeghi, A. Sendzik, A. Schulze, T. Mehner, H. Podlesak, D. Nickel, I. Scharf, T. Lampke

DOI: 10.12850/ISSN2196-0267.JEPT1645

LEUZE VERLAG
seit 1902

A new insight into the phosphorus distribution of nanocrystalline Ni-Ni_3P-diamond composites

D. Dietrich, A. Sadeghi, A. Sendzik, A. Schulze, T. Mehner, H. Podlesak, D. Nickel, I. Scharf, T. Lampke

Chemnitz University of Technology, Institute of Materials Science and Engineering, 09107 Chemnitz, Germany

The microstructure of an electroplated Ni-Ni_3P-diamond composite has been studied by field-emission scanning electron microscopy, energy dispersive X-ray spectrometry and transmission Kikuchi diffraction. The use of an electron transparent sample reduced the resolution limits of X-ray spectrometry and electron backscatter diffraction. Basing on the P distribution and Ni/Ni_3P orientation maps, standard observations made by backscattered electron imaging can be easily interpreted.

Keywords: Ni-P diamond coatings, phosphorus distribution, transmissions Kikuchi diffraction, electron backscatter imaging
Paper: Received: 2013-04-04 / Received in revised form: 2013-04-05 / Accepted: 2013-04-08

Introduction

Ni-P coatings are typical functional coatings used for corrosion and/or wear protection. Magnetic features and solderability are properties that have contributed to their application in electronics. Electroplated and electroless deposited Ni-P coatings show similar compositions, mechanical and electrochemical properties [1]. The majority of Ni-P deposits are obtained from the electroless process, an auto-catalytic chemical technique. Electroplated Ni-P is a good alternative since the deposition rate is not dependent upon a spontaneous chemical reaction and can be accelerated by current control. The relatively low working temperature permits milder operating conditions and is less energy intensive. Adding particles for composite deposition has been studied as an approach to modify the coating properties. Apart from diamond particles, Al_2O_3, SiC, Si_3N_4, CeO_2 and TiO_2 have been studied especially with respect to wear properties [2-8].

The phosphorus content in the nickel phosphorus alloy matrix of the composite can range between 2% to 20%, classifying them to low phosphorus coatings, medium phosphorus coatings and high phosphorus coatings. Depending on the phosphorus percentage, the structure of the as-deposited coating transforms from nanocrystalline (with decreasing grain size 10 nm to 2 nm) for 2%-12%P to amorphous with embedded 10 nm sized crystals for 10%-15%P and mostly amorphous with 12%-20%P [8, 10]. There was no indication observed of a sharply defined critical P content separating nanocrystalline and amorphous alloys. The as-plated microstructures and the transformation sequence during annealing have shown the same characteristics for both electroplated and electroless deposited alloys.

The thermal stability of the Ni-P alloy during annealing is remarkable compared to the lowered stability of other nanocrystalline materials and the understanding of the role of phosphorus

in solid solution and Ni_3P precipitation for grain growth inhibition is of high interest. Based on the conventional approach of grain boundary pinning by solute additions and second phase precipitations, some fundamental extensive microstructure characterisation has been published by HENTSCHEL et al. [10]. The authors concluded, that already in the as-plated state phosphorus is segregated at the grain boundaries with a concentration up to 11 at.%, in which the grains consist of a solid solution containing approx. 1 at.% P. During thermal treatment a transformation takes place that follows the sequence: Structural relaxation → P segregation and Ni (1%P) grain growth → Ni_3P-phase formation which is consistent with the Ni-P binary alloy phase diagram showing the equilibrium solid solubility of phosphorus in nickel as negligible. FÄRBER et al. [11] performed tomographic atom probe analyses and determined the three-dimensional P-distribution in electroless plated Ni-3.6 at.%P on an atomic scale. The authors defined an intercrystalline phase comprising grain boundaries and triple junctions where P segregation occurs. According to the determined grain sizes after heating up (11 nm at 250 °C and 25 nm at 400 °C), and assuming a metastable equilibrium, they successfully predicted grain sizes of other Ni-P alloys by a simple mass balance calculation at temperatures below Ni3P-formation. APACHITEI et al. [8] studied the effect of annealing on the structure of autocatalytic Ni-P and Ni-P-SiC coatings up to 500 °C. After continuous phosphorus segregation and a slight grain growth of Ni phase, approaching the metastable equilibrium at approximately 300 °C, the precipitation of the hard, semi-coherent NiP phase starts at approx. 400 °C. Bct Ni_3P and fcc Ni grains develop with increasing temperature. Their size was found to be 32 nm at 400 °C and 53 nm at 500 °C showing that solute (impurity) atoms or synthesis defects (porosity) retard the grain boundary movement in nanocrystalline alloys despite the high energy stored in the grains or boundaries. HUANG et al. [12] have shown the microstructure evolution with increasing P content and during heat treatment by using high resolution TEM (HR-TEM). Basing on these results the appearing hardening mechanisms of Ni–P alloys have been discussed.

It can be stated that a comprehensive understanding of the microstructure evaluation in Ni-P coatings during deposition and annealing is given in Ref. [8-12] and references therein. On this basis, the aim of this study is to demonstrate the microstructure of an annealed medium phosphorus diamond composite by different imaging methods based on field-emission scanning electron microscopy. The focus was filling the gap between micrometer-scale and nanometer-scale investigations by visualizing the phosphorus distribution in the fine-crystalline Ni-P matrix.

Experimental methods

Watts' electrolyte was used for electroplating under the deposition conditions 4 A/dm², 65 °C, pH 2.5, stirring agitation speed 500 rpm, and ultrasound agitation frequency 25 kHz.

Composed of the base chemicals 250 g/l $NiSO_4 \cdot 6\,H_2O$ (Sigma Aldrich), 30 g/l $NiCl_2 \cdot 6\,H_2O$ (Merck), 30 g/l H_3BO_3 (Merck), as phosphorus source 5 g/l $NaPO_2H_2 \cdot H_2O$ (Merck) and as surfactant 0.3 g/l $CH_3(CH_2)_{11}OSO_3Na$ (Riedel-de Haën) were added. A suspension of polycrystalline diamonds (Ø125 nm, 20 g/l) was prepared for particle incorporation. An annealing procedure (400 °C, 1 h) was established after deposition.

The phase ratio was examined by X-ray diffraction (XRD, D8 Discover, Bruker AXS) with Cu-K_α radiation (Cu-K_β filtering by Ni filter, beam diameter 1.2 mm).

For scanning electron microscopic (SEM) investigations a cross-section was prepared by cutting, hot mounting in electrically conductive resin, grinding and finally polishing with a colloidal silica solution. The used field-emission scanning electron microscope (FE-SEM NEON 40EsB, Zeiss) is equipped with a focused ion beam source (FIB) in cross-beam configuration and an energy dispersive X-ray spectrometer (EDS, EDAX Genesis). For secondary electron (SE) and backscatter electron (QBSD) imaging an excitation voltage of 5 kV respectively 10 kV was used, for scanning transmission electron microscopy (STEM) 30 kV.

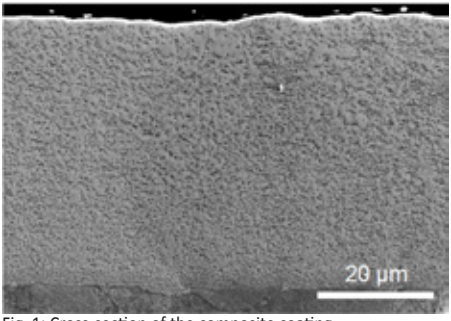

Fig. 1: Cross-section of the composite coating

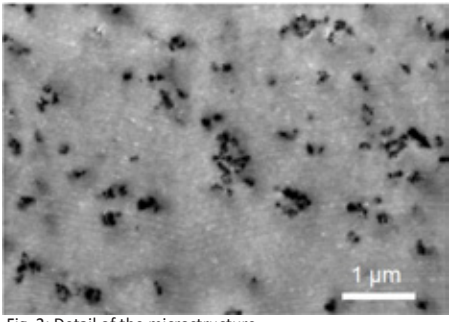

Fig. 2: Detail of the microstructure

Electron transparent samples were prepared using the FIB of the SEM and also examined in a transmission electron microscope (TEM, HITACH H8100, LaB_6 cathode) at 200 kV. Corresponding transmission Kikuchi diffraction (TKD) studies were done using the EBSD camera DigiView in the SEM operated at 25 kV in the high current mode with a 60 µm aperture and a step size of 15 nm and 5 nm. For data acquisition and analysis EDAX TSL OIM 5.31 comprising ChI scan software was used.

Results

A cross-section of the Ni-P-diamond coating is shown in *Figure 1* demonstrating a rather homogeneous diamond particle distribution. A detailed imaging reveals the formation of small agglomerates despite the application of ultrasound (*Fig. 2*). An electroplated Ni-diamond coating deposited under similar conditions shows remarkably lower particle agglomeration. The Ni-P matrix has a wavy lamellar structure, which can be observed by the compositional and crystal orientation contrast using the four-quadrant electron backscatter detector (*Fig. 2*).

The composition of the matrix (6.9 ± 1.0) at.%P has been determined by EDS corresponding to the XRD result revealing 62% Ni and 34% Ni_3P. A quantitative analysis on carbon was not possible because of the ambiguity of the quantification of light elements by EDS. Elemental mapping confirmed an inhomogeneous phosphorus distribution over the cross-section (*Fig. 3*). Inserted in this figure, the line scan shows vertical fluctuations of about 10% of the total P concentration which is also comparable to the mean deviation of the overall matrix composition. It should be noted that the thickness of the lamellas varies between 100 nm and some µm. The micron-sized variations have been observed frequently in electroplated and electroless deposited Ni-P coatings, for example in [1] and [13]. According to the deposition mechanism via oxidation of the sodium hypophosphite and reduction of the nickel ions,

$$NiSO_4 + NaPO_2H_2 + xH_2O \rightarrow Ni + 2H_{ads} + 2H^+ + SO_4^{2-} + NaH_2PO_3 \quad (1)$$

$$2NaPO_2H_2 + 2H_{ads} \rightarrow NaH_2PO_3 + P + NaOH + xH_2O \quad (2)$$

$$3NaH_2PO_2 + NiSO_4 + xH_2O \rightarrow Ni + P + 2H^+ + Na^+ + SO_4^{2-} + 2NaH_2PO_3 \quad (3)$$

the incorporation of phosphorus in the deposit depends on the pH, i.e., proton concentration. Therefore, local pH variations cause the variation in the deposit phosphorus content.

The fine variations of about 100 nm, which reveal the compositional contrast in conjunction with the crystal orientation contrast (*Fig. 2*) seem to be connected with the precipitation and crystal formation of both phases in the Ni-P matrix. To get a deeper insight an electron transparent lamella was prepared with a position shown in *Figure 4*.

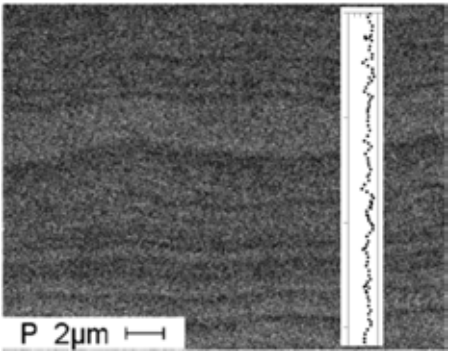

Fig. 3: Phosphorus distribution in the cross-section and vertical P line scan

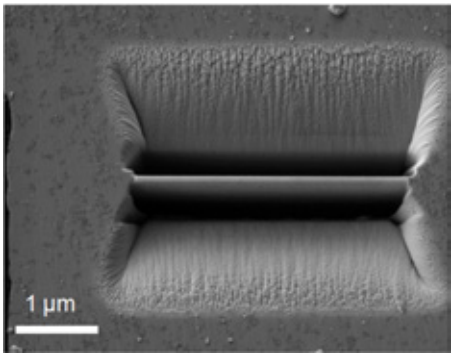

Fig. 4: TEM lamella position in the cross- section with the coating surface left

Electron diffraction (*Fig. 5, left*) reveals a large number of frequently bright spots on the (111), (200) and (220) rings of the diffraction pattern of polycrystalline nickel and weaker spots on the (321), (112) and (141) rings corresponding to polycrystalline Ni_3P. The circle in the diffraction pattern demonstrates the aperture placed to receive the dark field (DF) image corresponding to the bright field (BF) image in *Figure 5*. A variation of the crystal size in the range of few tenth of nanometres can be observed (*Fig. 5, 6 and 7*), which is in agreement with the XRD results revealing a mean size of 47 nm for Ni and of 39 nm for Ni_3P grains. The XRD lattice parameter evaluation resulted in the mean lattice parameters a = 0.35300 nm for the fcc Ni phase and a = 0.8964 nm and c = 0.4395 nm for the bct Ni_3P phase which is comparable to the results of SUI et al. [14] taking into account different lattice strain conditions.

Compared to the grain size of the Ni and Ni_3P crystals, the prepared TEM lamella is not thin enough (mostly thicker than 100 nm). Some grains are lying upon each other thus causing blurred appearance of the TEM BF images (*Fig. 6*). Nevertheless, a good bonding of the diamond particles to the matrix can be stated (*Fig. 7 and 8*). A rounded diamond particle in the matrix with facetted Ni and Ni_3P crystals is shown by high-resolu-

tion TEM imaging (*Fig. 8*). The overlapping matrix grains reveal parallel and rotational moiré fringe patterns. There is evidence for embedded H_2 pockets in the dark grain indicated by arrows; nevertheless, this was an occasional observation.

of the nanocrystals which form the Ni-P matrix. Recently, the application of transmission Kikuchi diffraction (TKD) has been established reducing the resolution limit to one or two orders of magnitude [17, 18]. The application of this technique

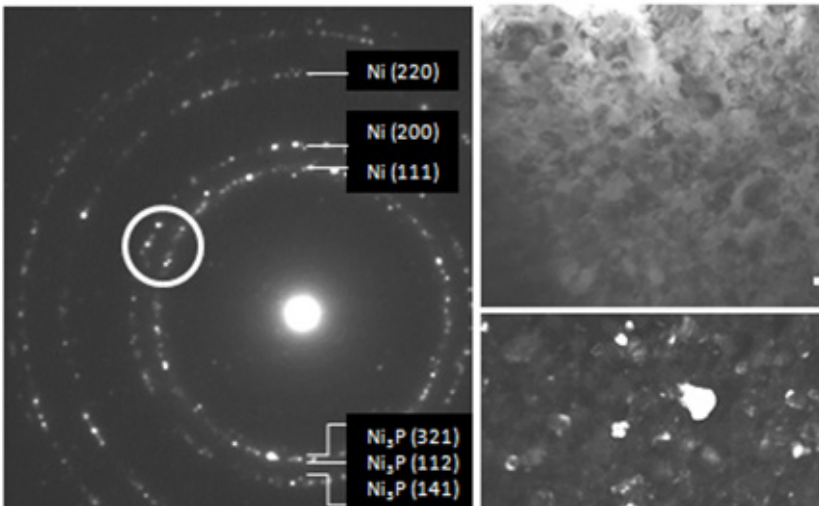

Fig. 5: Electron diffraction pattern (left), corresponding bright (upper right) and dark field image

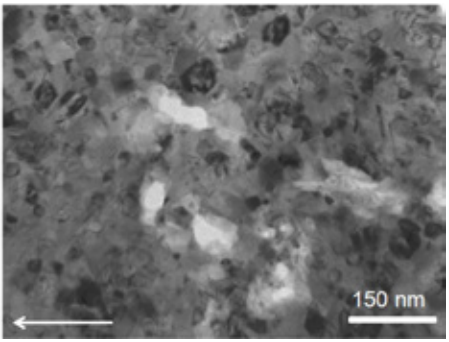

Fig. 6: Diamond agglomerate in Ni-P matrix (arrow – deposition direction)

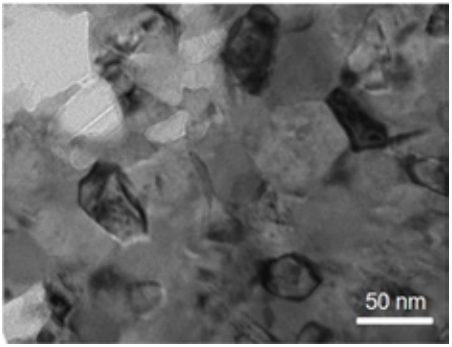

Fig. 7: Diamond particles with proper matrix bonding

The characterization of electroplated Ni composites has been done successfully by means of electron backscatter diffraction (EBSD) thus revealing grain size and texture of the nickel matrix [15, 16]. The practical resolution is in general above the size

requires an electron transparent lamella. The diffraction patterns are acquired from behind the sample. Accordingly, the TKD technique is sometimes referred to as t-EBSD, particularly since the conventional EBSD design in the SEM can be used.

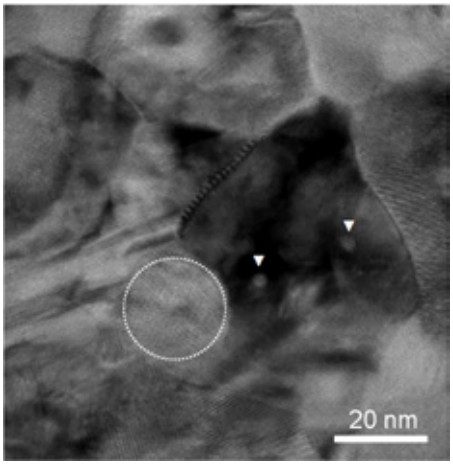

Fig. 8: High resolution TEM image showing a diamond particle between facetted Ni/Ni_3P grains, arrows indicate gas pockets

forescatter electron detector (FSD) of the EBSD unit (comparable to the QBSD of the SEM). The inserted carbon map shows the region of interest for comparison with the phosphorus map both acquired with a step size of 15 nm. The insert in the phosphorus map (green box in *Fig. 9*, upper row) is shown below with the corresponding pattern quality map and nickel orientation maps acquired with a step size of 5 nm. The quality map does not reveal grain boundaries. Due to the relative thickness of the lamella compared to the grain size as mentioned above, some grains are lying upon each other thus contributing to mixed TKD patterns. Therefore, the confidence of the pattern indexing is reduced and only single large grains can be detected with a reasonable confi-

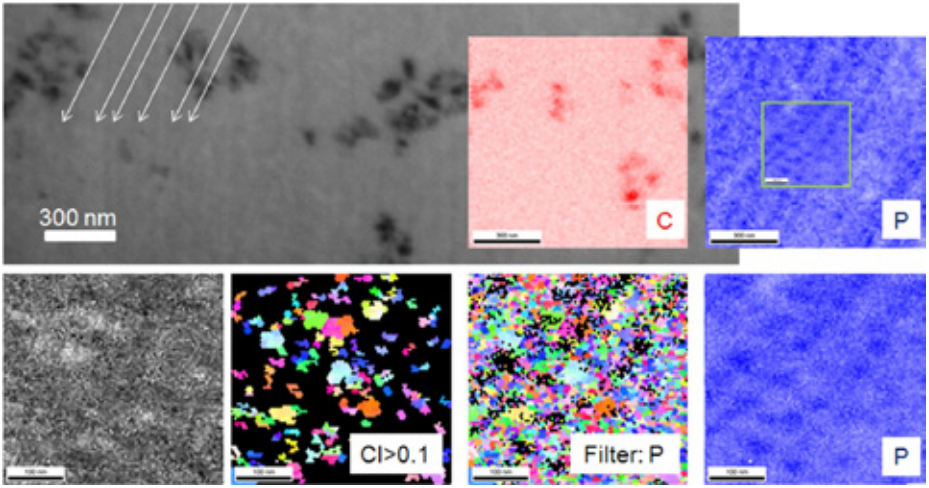

Fig. 9: TKD and EDS results
Upper row (step size 15 nm, scale bar 300 nm): FSD image (arrows indicate lamellas with P fluctuations), inserted carbon map and corresponding phosphorus map (the green box marks the position of the maps in the lower row)
Lower row (step size 5 nm, scale bar 100 nm): pattern quality map, Ni orientation map (CI > 0.1), Ni orientation map (Filter low P concentration), phosphorus map

The investigation of the lamella prepared by FIB, made it possible to get some more insight into the Ni-P matrix. *Figure 9* shows a small region of the TEM lamella with some diamond agglomerates using the atomic number contrast revealed by the dence. Such grains are shown in the Ni orientation map filtered with a confidence index CI > 0.1, commonly accepted for cubic structures. Another Ni orientation map has been calculated with a filter derived from the phosphorous EDS signal

shown in the corresponding phosphorus map thus blanking possible contributions of Ni_3P crystals.

sequences of Ni and Ni_3P grains by dotted lines. The mostly larger Ni grains and the comparatively smaller Ni_3P grains form lamellas with varying P

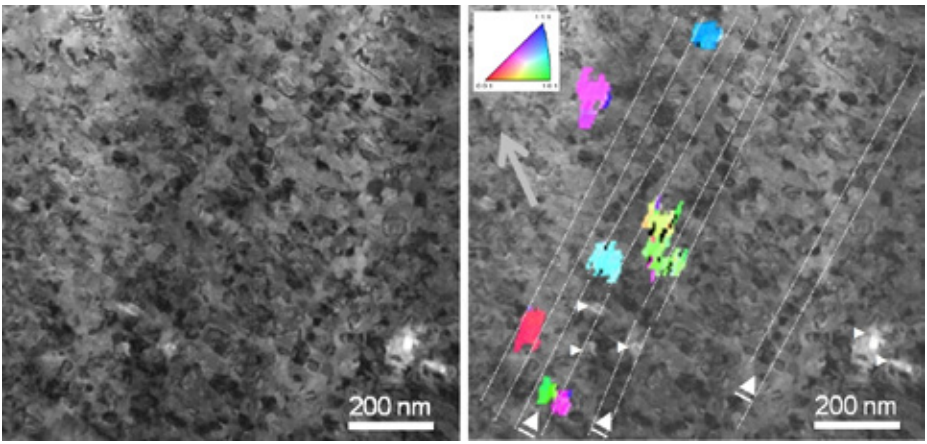

Fig. 10: TEM bright field image of the Ni-P composite (left) and with indication of the growth direction (grey arrow), some diamond particles (small triangles), some sequences of Ni and Ni_3P grains (dotted lines, larger triangles indicate P rich regions) and some orientation colour-coded Ni grains (right)

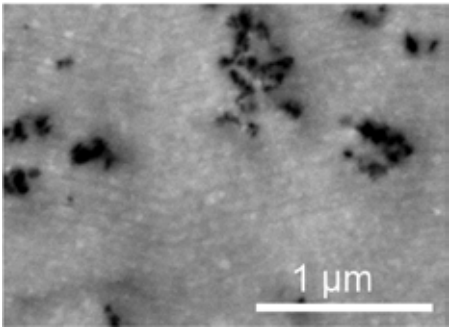

Fig. 11: QBSD image, detail of *Fig. 2*

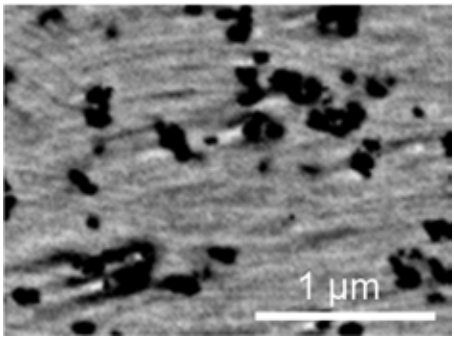

Fig. 12: QBSD image after carbon-coating

The maps demonstrate sequences of Ni and Ni_3P crystals and facilitate the interpretation of the TEM bright field images. Some Ni grains with reasonable confidence are shown as an overlay with their colour-coded orientation according to the stereographic triangle in the corresponding TEM image (*Fig. 10*). Additionally this figure contains indications which are given for some diamond particles by white triangles and for some

concentration. These are consecutive fronts of precipitation and crystallisation which are roughly built upwards in the growth direction of the composite coating. Deviations from the perpendicular direction are usual and due to the undulate appearance of the lamellas.

Accordingly, the observations in the backscattered electron images (*Fig. 2, Fig. 11*) can be supported.

The bright dots indicate crystals in an appropriate orientation for electron backscattering. The dark lines can be interpreted as consecutive fronts of precipitation and crystallisation. This can be observed only on a sample with a well-prepared clean surface. A carbon coating deposited to prevent sample charging inhibits the evidence of the orientation contrast. In this case the composition contrast remains separated and shows the Ni_3P crystals as tiny black spots (*Fig. 12*).

Conclusion

The understanding of the properties of Ni-P coatings and Ni-P composites can be related to their phosphorus content and microstructure. This has been done during the last decades by electron microscopy and in more detail by fundamental research tools like atom-probe field-ion microscopy. The aim of this paper was to fill the gap between micrometer-scale and nanometer-scale investigations by visualizing the phosphorus distribution in the fine-crystalline Ni-P matrix. The application of analytical methods based on field-emission scanning electron microscopy on an electron-transparent sample of an annealed medium phosphorus diamond composite has been demonstrated and gives an instructive insight into the phosphorus distribution. Basing on P distribution and Ni/Ni_3P orientation maps, standard observations made by backscattered electron imaging in the SEM can be understood.

References

[1] P. Peeters, G.v.d. Hoorn, T. Daenen, A. Kurowski, G. Staikov. Properties of electroless and electroplated Ni–P and its application in microgalvanics. Electrochim Acta 47 (2001) 161–169

[2] Y. de Hazan, D. Werner, M. Z´graggen, M. Groteklaes, T. Graule. Homogeneous Ni-P/Al_2O_3 nanocomposite coatings from stable dispersions in electroless nickel baths. J Colloid Interf Sci 328 (2008) 103-109

[3] M.-C. Chou, M.-D. Ger, S.-T. Ke, Y.-R. Huang, S.-T. Wu. The Ni–P–SiC composite produced by electro-codeposition. Mater Chem Phys 92 (2005) 146–151

[4] K.-H. Hou, W.-H. Hwu, S.-T. Ke, M.-D. Ger. Ni–P–SiC composite produced by pulse and direct current plating. Mater Chem Phys 100 (2006) 54–59

[5] J. Alexis, B. Etcheverry, J.-D. Béguin, J.-P. Bonino. Structure, morphology and mechanical properties of electrodepositedcomposite coatings Ni–P/SiC. Mater Chem Phys 120 (2010) 244-250

[6] B. Bozzini, M. Boniardi, A. Fanigliulo, F. Bogani. Tribological properties of electroless Ni-P/diamond composite films. Mater Res Bull 36 (2001) 1889–1902

[7] J.N. Balaraju, T.S.N. Sankara Narayanan, S.K. Seshadri. Structure and phase transformation behaviour of electroless Ni–P composite coatings. Mater Res Bull 41 (2006) 847–860

[8] I. Apachitei, F.D. Tichelaar, J. Duszczyk, L. Katgerman. The effect of heat treatment on the structure and abrasive wear resistance of autocatalytic NiP and NiP–SiC coatings. Surf Coat Techn 149 (2002) 263–278

[9] S.C. Mehta, D.A. Smith, U. Erb. Study of grain growth in electrodeposited nanocrystalline nickel-1.2 wt.% phosphorus alloy. Mater Sci Eng A204 (1995) 227-232

[10] T. Hentschel, D. Isheim, R. Kirchheim, F. Müller, H. Kreye. Nanocrystalline Ni±3.6 at.% P and its transformation sequence studied by atom-probe field-ion microscopy. Acta mater. 48 (2000) 933-941

[11] B. Färber, E. Cadel, A. Menand, G. Schmitz, R. Kirchheim. Phosphorus segregation in nanocrystalline Ni±3.6 at.% P alloy investigated with the tomographic atom probe (TAP). Acta mater 48 (2000) 789-796

[12] H.-C. Huang, S.-T. Chung, S.-J. Pan, W.-T. Tsai, C.-S. Lin. Microstructure evolution and hardening mechanisms of Ni–P electrodeposits. Surf Coat Techn 205 (2010) 2097–2103

[13] C. S. Lin, C. Y. Lee, F. J. Chen, W. C. Li. Structural Evolution and Internal Stress of Nickel-Phosphorus Electrodeposits. J Electrochem Soc, 152 (2005) C370-C375

[14] M. L. Sui, K. Lu. Variation in lattice parameters with grain size of a nanophase Ni_3P Compound. Mater Sci Eng A179/180 (1994) 541-544

[15] D. Thiemig, A. Bund, D. Dietrich, T. Lampke. Characterization of the Particle Incorporation Behaviour and the Microstructure of electrocodeposited Ni-Al_2O_3 Nanocomposites, JEPT - Journal of Electrochemistry and Plating Technology, Online journal, doi: 10.12850/ISSN2196-0267.JEPT513

[16] T. Lampke, B. Wielage, D. Dietrich, A. Leopold. Details of crystalline growth in co-deposited electroplated nickel films with hard (nano)particles. Appl Surf Sci 253 (2006) 2399-2408

[17] R.R. Keller, R.H. Geiss. Transmission EBSD from 10 nm domains in a scanning electron microscope. J Microsc, 245 (2011) 3, 245–251, doi: 10.1111/j.1365-2818.2011.03566.x

[18] P.W. Trimby Orientation mapping of nanostructured materials using transmission Kikuchi diffraction in the scanning electron microscope. Ultramicroscopy 120 (2012) 16 - 24, doi: 10.1016/j.ultramic.2012.06.004

Corresponding author:

Dr. rer. nat. Dagmar Dietrich
Institute of Materials Science and Engineering, Chemnitz University of Technology, 09107 Chemnitz, Germany

Authors:

M.Sc. Amir Sadeghi
Institute of Materials Science and Engineering, Chemnitz University of Technology, 09107 Chemnitz, Germany

Dipl.-Phys. Andrea Sendzik
Institute of Materials Science and Engineering, Chemnitz University of Technology, 09107 Chemnitz, Germany

Dipl.-Ing. Anne Schulze
Institute of Materials Science and Engineering, Chemnitz University of Technology, 09107 Chemnitz, Germany

Dipl.-Phys. Thomas Mehner
Institute of Materials Science and Engineering, Chemnitz University of Technology, 09107 Chemnitz, Germany

Dr. rer. nat. Harry Podlesak
Institute of Materials Science and Engineering, Chemnitz University of Technology, 09107 Chemnitz, Germany

Dr.-Ing. habil. Daniela Nickel
Institute of Materials Science and Engineering, Chemnitz University of Technology, 09107 Chemnitz, Germany

Dr. rer. nat. Ingolf Scharf
Institute of Materials Science and Engineering, Chemnitz University of Technology, 09107 Chemnitz, Germany

Prof. Dr.-Ing. habil. Thomas Lampke
Chair of Surface Technology/ Functional Materials, Chemnitz University of Technology, 09107 Chemnitz, Germany

CONTACT:

EUGEN G. LEUZE VERLAG KG
Ralf Schattmaier
Karlstraße 4
88348 Bad Saulgau
Germany

Email: ralf.schattmaier@leuze-verlag.de
Phone: +49 0 7581 4801-12
Fax: +49 0 7581 4801-10